Copyright Notice

Train-side Passive Magnetic Measurements

Oliver Heirich, Benjamin Siebler
DLR (German Aerospace Center)
Institute of Communications and Navigation
82234 Wessling-Oberpfaffenhofen, Germany
{firstname.lastname}@dlr.de

***Abstract*—Passive magnetic sensors can measure the magnetic field density in three orthogonal axes and are often integrated on a single chip. These sensors are low-cost sensors and widely used in car navigation as well as in battery powered navigation equipment such as smartphones. There, its general purpose is the measurement of the heading angle by an electronically gimbaled compass technique. We are interested in train localization with multiple, exclusively onboard sensors and a track map. This approach is considered as a base technology for future railway applications such as train-centric train control, collision avoidance systems and autonomous driving. It has been shown that active magnetic measurements, such as a metal detector, is very beneficial for onboard train localization.**

We are interested in the question: How beneficial are passive magnetic measurements for railway navigation?
In this paper we present and analyze magnetic measurements recorded on a regional train at regular passenger service. We present promising correlations of the measurements with the train speed, track positions and the traveled switch way. We further present and analyze a conventional magnetic compass approach for railways.

I. Introduction

Train localization with multiple, exclusively onboard sensors and a track map is considered as a base technology for future railway applications, such as train-centric train control, collision avoidance systems and autonomous driving. Train localization is a safety-of-life application, so there is a focus on accuracy for the correct, track-selective train position, but also the need of robustness in terms of redundancy. Therefore, onboard train localization is often addressed by multi-sensor approaches [1],[2],[3]. These approaches could be extended with passive magnetic methods for additional accuracy and redundancy.

Magnetic sensors such as AMR (Anisotropic magneto-resistance, [4]) sensors can measure in 3-axis and are integrated on a single chip. AMR sensors are low-cost sensors and widely used in vehicular and marine navigation as well as in battery powered handheld navigation equipment such as smartphones. These sensors are often integrated in combination with accelerometers or an IMU (Inertial Measurements Unit) and its general purpose is the measurement of the yaw angle by an electronically gimbaled compass technique [5].

Compass approaches typically tend to suppress the effects of different magnetic fields than the earth field, which are often denoted as distortions. The magnetic fields in special environments can have its own, special signature. This characteristic is very beneficial for localization applications, as shown in [6] for indoor environments. A vehicle and also the environment of the vehicle can be described with a of set magnetic dipoles. In [7], passive magnetic measurements on fixed positions are used to identify moving vehicles and directions.

An active magnetic sensor for trains, called the eddy current sensor is specified in [8] and used for train localization in [9],[10]. This sensor is a special metal detector onboard a train and detects railway specific track components, such as sleepers and elements of the switch. It can further infer the traveled switch way [10]. In these approaches, the eddy current sensor contains coils for a modulated magnetic field generation and other coils for a differential measurement of the resulting field affected from metallic structures in the vicinity.

We propose a measurement setup as shown in Fig. 1, where the IMU with integrated magnetometer can be seen (orange box) in the opened protection case. We present and analyze

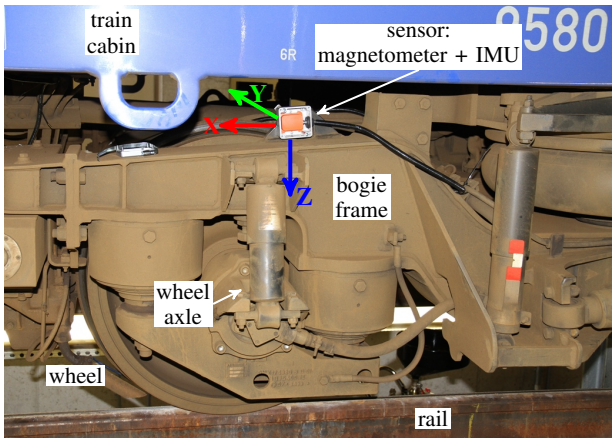

Fig. 1. Magnetic measurement setup on the front bogie of a regional train.

passive magnetic measurements in three axes, recorded on a regional train at regular passenger service. These measurements are considered passive, as it uses no active generated (static or modulated) magnetic field for sensing. This sensor measures only the instantaneous magnetic field as it is superimposed from dipoles in the environment. We analyze and show correlations of magnetic measurements with focus on the train localization application.

II. Railway Navigation Application

We want to utilize the passive magnetic measurements for onboard railway localization with a probabilistic multi-sensor approach [11]. A position in railway localization is usefully expressed in topological coordinates, which is the track ID R and the metric 1-D position s on that track. The topological position addresses a position in a railway network

unambiguously. Further, a train frame to track direction (dir) is needed, as a train can be placed in two possible, opposite directions on a track. This is important to translate frame definitions for frame dependent sensors, such as the three axis magnetic field sensor or inertial sensors. At last, the actual train speed ($\dot{s}$) is an important information. The complete state vector of train localization is a set of unknown, hidden variables:

$$T = (R, s, dir, \dot{s}). \tag{1}$$

The goal for train localization is to resolve T with data filters based on sensor fusion techniques for combining different sensor measurements.

In this paper, the question is, how can the magnetic field contribute to onboard train localization by direct measurement or indirect observation of these variables.

III. Magnetic measurements

The sensor measures the magnetic field strength $\vec{B}$ in three dimensions. In the railway environment, there are superpositions of the magnetic field expected from several magnetic dipoles: the magnetic earth field and from ferro-magnetic material such as as rails, trains, or other metallic infrastructure. Further, there are alternating fields from AC power lines, engines, signaling and ferromagnetic material moving relative to the sensor.

A. Measurement Frame

We consider the magnetic measurements in the train frame, as shown in Fig. 1:

- X: longitudinal train axis pointing to train front
- Y: lateral train axis pointing to the right side
- Z: vertical train axis pointing down

As the sensor measures in the sensor frame, a rotation of the measurement vector $\vec{B}$ is needed:

$$\vec{B}^{\text{train}} = \mathbf{C}^{\text{train}}_{\text{sensor}} \cdot \vec{B}^{\text{sensor}}. \tag{2}$$

The rotation matrix $\mathbf{C}^{\text{train}}_{\text{sensor}}$ is a direction cosine matrix (DCM) and can be calculated by Euler angles of roll, pitch and yaw between sensor and train frame.

B. Spatial Transformation

The measurements are recorded sample by sample in the temporal domain with a constant frequency of $200\,\text{Hz}$. We are interested in location dependent correlations of the measurements and the railway environment. Within one track, the railway localization problem is one dimensional and signals or features can be addressed in the metric, spatial domain. The transformation of the magnetic signal from time to spatial domain (i.e. seconds to meters) is achieved by the change of positions, respective the train speed. For our transformations we use directly the GNSS (Global Navigation Satellite System) speed measurement of the PVT (position, velocity, time) output of a GNSS receiver. The transformation of the time signal y_t with time samples x_t to the spatial signal y_s with metric position samples x_s is simply a linear data interpolation:

$$y_s = f_{interp}(x_t, y_t, x_s). \tag{3}$$

For the metric location samples, we consider a vector of equally spaced samples of $0.1\,\text{m}$.

C. Temporal Spectrogram

This plot is achieved by the following steps by well known signal processing methods [12]:

1) First, the measurements are divided in sequences of N samples. At a fixed sampling rate f_s, the sequences have a length of $N \cdot f_s$ seconds.
2) The second step calculates the power spectral density (PSD) of each sequence.
3) The plot displays all PSDs as columns and each column is a point in time corresponding with its measurement sequence.

A larger sequence and larger FFT (fast Fourier transform) is favorable in frequency resolution, but a larger sequence relates also to lower time resolution. For good frequency resolution and a smoothed time resolution, it is possible to overlap the sequences by a certain number of samples.

D. Speed Spectrogram

The speed spectrogram shows the power spectral density (PSD) in frequency over different speeds. The processing is similar to the temporal spectrogram except of the last step: Here, each PSD is sorted by its mean GNSS speed of the sequence in a speed bin. These speed bins have a certain width (e.g. in km/h). In the case a bin contains multiple PSDs, an average PSD is computed.

IV. Magnetic Compass

The magnetic compass is a very common and well known navigation technique based on passive magnetic measurements. In general, a magnetic compass measures the angle to magnetic north from the horizontal part of the magnetic earth field [5]. An electronic compass measures the magnetic field in three dimensions, rotates the measurements to horizontal plane and calculates the angle to magnetic north. Declination δ is the deviation of angle of magnetic north to true north and inclination λ is the angle of the magnetic vector to the horizontal. These angles and the local earth field strength $|B|$ are dependent on the position and can be computed from magnetic earth field models [13]. The expected magnetic earth field in train frame on a specific position is:

$$\begin{pmatrix} B_x \\ B_y \\ B_z \end{pmatrix} = \begin{pmatrix} \cos(\psi + \delta) \cdot \cos(\lambda) \\ \sin(\psi + \delta) \cdot \cos(\lambda) \\ \sin(\lambda) \end{pmatrix} \cdot |B^{\text{earth}}|. \tag{4}$$

A. Compass Computation

In a first step, the hard iron offset of all three axes are compensated by:

$$\vec{B}^{\text{cal,train}} = \vec{B}^{\text{train}} - \vec{m}^{\text{hard}}. \tag{5}$$

If the train frame is inclined to the horizontal plane by a roll angle ϕ and a pitch angle θ, the measurement vector is rotated to the horizontal by the DCM:

$$\vec{B}^{\text{cal,hor}} = \underbrace{\begin{pmatrix} \cos\theta & \sin\phi\sin\theta & \cos\phi\sin\theta \\ 0 & \cos\phi & -\sin\phi \\ 0 & 0 & 0 \end{pmatrix}}_{\mathbf{C}_{\text{train}}^{\text{horizonal}}} \cdot \vec{B}^{\text{cal,train}}. \quad (6)$$

The magnetic yaw angle is computed from the calibrated and horizontal values:

$$\psi^{\text{mag}} = \arctan\left(\frac{B_y^{\text{cal,hor}}}{B_x^{\text{cal,hor}}}\right). \quad (7)$$

Finally, the true north yaw angle is computed by magnetic north and the declination:

$$\psi = \psi^{\text{mag}} - \delta. \quad (8)$$

B. Calibration

There are hard iron and soft magnetic effects which superimpose the earth field and cause a different compass angle than the desired angle to north [5]. We consider static, hard iron calibration as a time-persistent offset of the measurements resulting from the train and the tracks. We are able to calibrate our magnetic measurements with GNSS heading measurements to true north and the knowledge of the local declination. As shown in the compass computation, only a ratio of the lateral and longitudinal field is needed. The calibration procedure includes a data fit by least squares method of measurements and expected measurement of the GNSS heading:

$$a_x \cdot B_x + m_x = \cos(\psi_{\text{GNSS}} + \delta), \quad (9)$$
$$a_y \cdot B_y + m_y = \sin(\psi_{\text{GNSS}} + \delta). \quad (10)$$

The offsets m_x and m_y are influenced by nearby hard magnetic dipoles and correction is needed for correct compass computation. The inclination calibration is not required, as the compass equation (7) computes only a ratio.

V. Magnetic Data Set

The measurements were recorded on the passenger train "Alstom Coradia Lint41" at regular passenger service conditions. In Fig. 2 the train speed and the occurring switches (split left, right or merge) are shown for an example run from Augsburg main station to Friedberg.

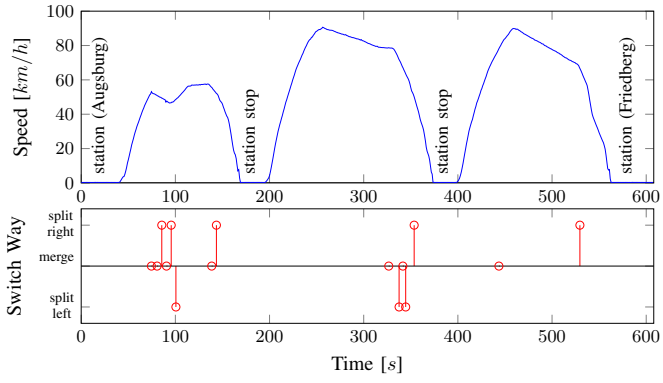

Fig. 2. [Top] train speed over time, [bottom] traveled switch ways.

The data set contains 200 Hz magnetic measurements on the front bogie from a Xsens MTi sensor and a GPS data from a Ublox LEA 6T receiver. The Xsens sensor system is based on low-cost sensor elements, such as the magnetic sensor HMC1053 from Honeywell. For the compass analysis, a second sensor (Xsens MTi sensor) was placed inside the train driver's cab. The wheels had a circumference of 2420 mm, i.e. a diameter of 770 mm. Figure 3 shows the magnetometer data

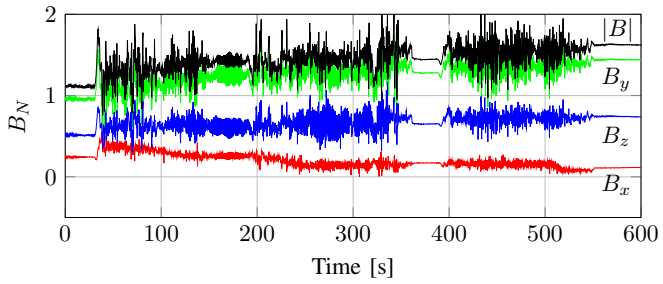

Fig. 3. Magnetic measurements of 3 axis and magnitude over time.

and the magnitude of the same train run in the unit of normalized earth field B_N. The signal of the magnitude indicates different magnetic dipoles and/or modulated magnetic fields depended over time.

VI. Analysis

A. Temporal spectrogram

In Fig. 4 the temporal spectrogram of the longitudinal x-axis is shown. The spectrogram of the y and z axis look very similar and are not shown here. The spectrogram uses a sequence and FFT length of 512 samples, and one data sequence with $f_s = 200$ Hz has a length of 2.56 s. From the

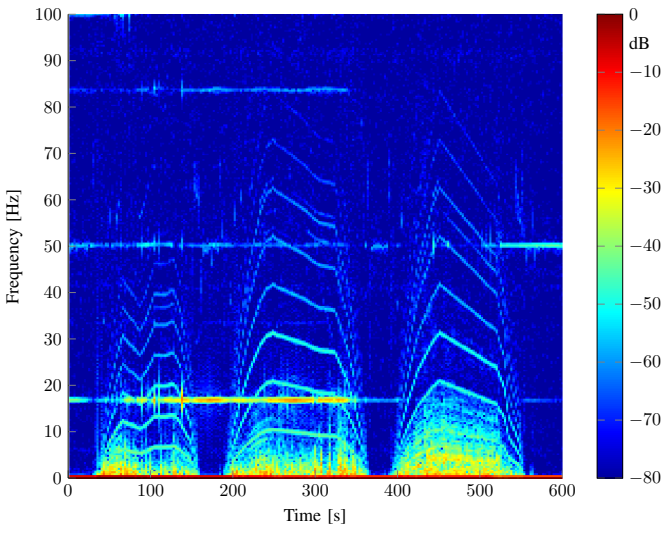

Fig. 4. Spectrogram over time of magnetic x-axis signal.

spectrogram, we can see horizontal, time independent lines. The strongest signal is at the 0 Hz line and possibly caused by hard magnetic materials of train or tracks and the earth

field. The lower line is correlated with German railway AC power of 16.7 Hz, the middle with 50 Hz of general AC power modulation and/or second harmonic of railway power. Other, weak lines can be identified at higher harmonics of the railway power, e.g. at first harmonic 33.4 Hz and also at the forth harmonic 83.5 Hz.

The measured train was Diesel powered, so the measured electrical current in the power lines were caused by electrical trains operating in the same grid. There are clearly velocity dependent frequencies, as the signal shape of the speed profile of Fig. 2 is repeated by multiple times.

B. Speed

Figure 5 shows the correlation of speed and the magnetic spectrum. The parameters are 512 for the window and FFT size, the speed resolution is km/h. There are clear linear relations (lines) between speed and frequency in this speed spectrogram. These lines correspond to the wheel circumference of 2.42 m (770 mm in diameter). The resulting frequency of the n-th harmonic f_n is calculated with the diameter d and the speed v in km/h by this model:

$$f_n = \frac{v}{3.6 \cdot d \cdot \pi} \cdot (n+1). \tag{11}$$

The black, dashed lines show this model up the 6-th harmonic. Further harmonics can be seen with aliasing effects in the upper right corner.

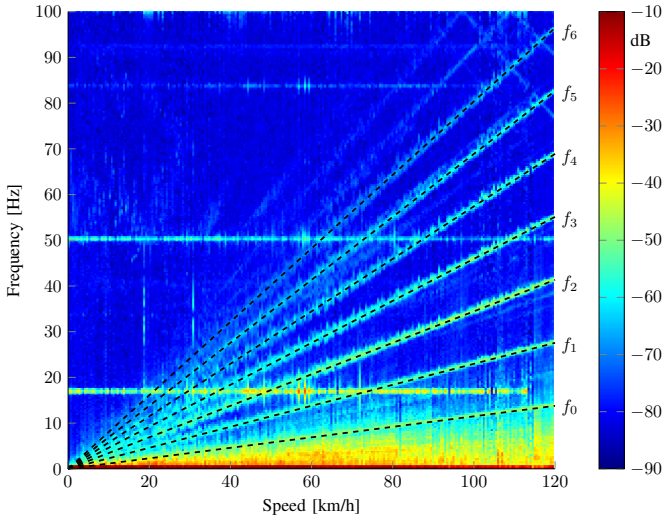

Fig. 5. Signal spectrum over train speed.

C. Track Position

In Fig. 6 the magnetic signals of two *different* train runs over the *same tracks* are shown. The signals are low pass filtered to suppress other effects as the wheel and power line. The filter is a 6th-order Butterworth filter (maximal flat response at passband) with a cut-off frequency of 1 Hz. Then the signals are translated from time to spatial domain. Both signals of the different runs are highly correlated by the position, as both signals are very similar for same distance from a common start point. The railway environment has a very significant magnetic characteristic (or code) dependent

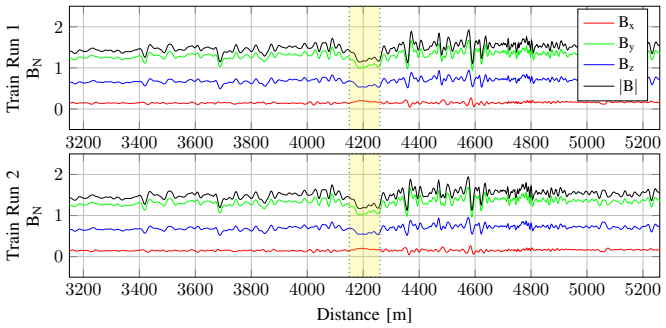

Fig. 6. Spatial magnetic signals of two different runs over the same track.

on position. The yellow marked area refers to the position and length of the metallic railway bridge shown in Fig. 7. This metal structure is a landmark in the railway environment and characterized by a lower total field magnitude and less variation than other positions.

Fig. 7. Metallic railway bridge from train driver's perspective.

D. Railway Switch

Fig. 8 shows magnetic signals of two different runs, starting from the same track and traveling over different switch ways. The switch is shown in a satellite image in the middle and

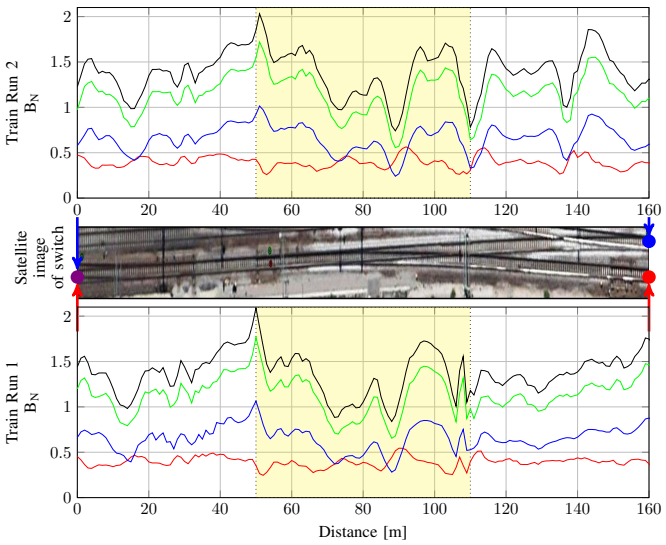

Fig. 8. Signals of the same switch from different switch way runs. [Satellite image: Google Earth]

aligned to the x-axis of the data graphs. The train traveled the split-switch two times (from left to right in the figure) with forward motion, and the sensor was mounted on its right side (pointing to upper side in figure). The yellow areas indicate approximately the switch, starting from the switch rails to the switch frog (position where the inner rails cross and split). It can be seen, the signals are very similar in both runs until the middle of the switch (yellow area). The signals after the switch frog shows clearly differences between the two runs on different switch ways.

VII. Application: Railway Compass

A theoretic consideration of a railway compass application might result in doubts about feasibility and quality due to the ferro-magnetic materials in the railway environment. Nevertheless, we show the performance of such a railway compass as it is from real sensor data. The local magnetic field values for the start point of declination, inclination and total field strength are obtained from a magnetic model [13]:

$$\delta = 2.35°, \quad (12)$$

$$\lambda = 64.33°, \quad (13)$$

$$|m| = 48.254\mu T. \quad (14)$$

The data set for the magnetic compass is a longer train run in order to achieve as many different yaw angles as possible for a calibration. The results shown are processed from a secondary synchronized sensor mounted inside the train driver's cab. The compass result is shown in Fig. 9 as well as the GNSS heading measurements as reference.

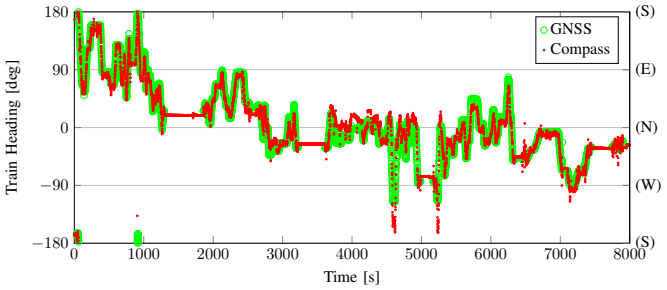

Fig. 9. Magnetic Compass heading (sensor: **train driver's cab**) and GNSS heading measurements.

The comparison of GNSS heading and compass heading of train driver's cab from Fig. 9 is shown in the upper plot of Fig. 10. The red lines indicate $\pm 90°$ degree difference which is the criterion for correct semi-circle detection. Data gaps are related to train stops, in which the GNSS receiver can not output a heading angle of a zero motion vector. The cabin mounted compass can be used to measure the direction of the train frame to a defined track frame, which is only two possibles angles separated by $180°$. The maximum error of train diver's cab compass of this data set is $59.0°$, the empirical deviation is $11.0°$. The bogie mounted sensor is not suitable for a coarse direction measurement, as seen in the bottom plot of Fig. 10. The bogie mounted sensor has shown strong position dependent signals in the previous plots. The y-axis contains a stronger position dependency signal than the x-axis (see Fig. 6 or Fig. 8). This is disadvantageous for compass computation, as these axes are affected differently and a ratio is calculated.

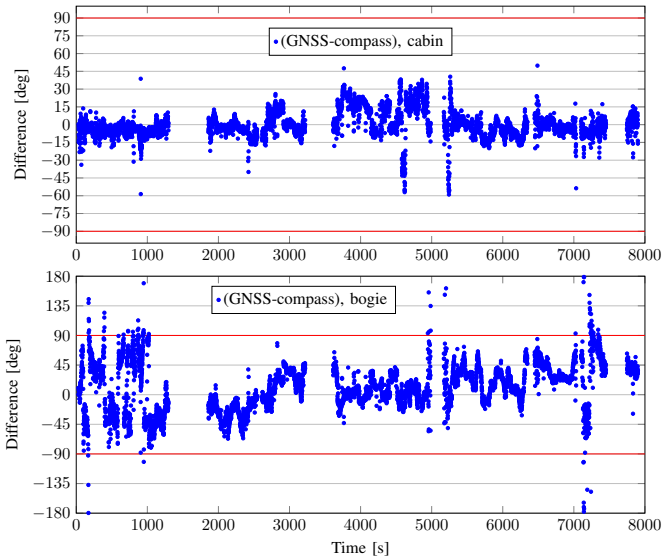

Fig. 10. Comparison of GNSS heading and compass angle from: [Top] **train driver's cab** magnetometer [Bottom] **bogie** magnetometer.

VIII. Discussions

From the presented measurements and analysis, we can derive further use for the train localization application.

A. Track position

The low-pass filtered magnetic signals of B_x, B_y, B_z and magnitude $|B|$ show a significant position dependency and are suitable for the observation of the 1-D track position s. A correlation technique seems very promising in resolving the position. This can be integrated in a technical train localization approach in combination with prior recorded signals, stored in an electronic map.

B. Track and switch way

The characteristic signal of the track position analysis is also suitable for identification of different tracks. The switch analysis showed different signal for the competing switch ways. This is considered as a real benefit for train localization with the need for track-selective accuracy. However, for switch elements detection, the passive magnetometer at the presented bogie position has not the high signal resolution of switch elements or sleepers compared to the active magnetic eddy current sensor [10].

C. Train frame direction

The cabin sensor showed promising results for the direct and especially initial frame direction measurement. The bogie mounted sensor shows a high position dependent correlation in y and z axis, but less in x axis. This fact is less beneficial for compass angle computation.

D. Train speed

As there is a correlation between wheel turns and magnetic measurements (Fig. 5), a suitable method [14] may infer the train speed. This speed measurement can be considered as

a stand-alone application itself or as a contribution to train localization. The measurements look very promising for further speed computation from all axis and magnitude. We propose also further use as a wheel size monitoring application for diagnostics from known speed.

IX. Conclusions and Outlook

We analyzed real magnetic measurements from a regional train in terms of relevance for the train localization application. The main benefits of magnetic chip sensors are the small size, low power and low cost.

We could show, that there is a significant correlation between train speed, wheel diameter and magnetic measurements, which is ideal for a speed sensor application. The magnetic information dependent on position is very beneficial for train localization. We consider it complimentary to GNSS measurements, as satellite reception is poor or not available in stations with metallic roofs, below bridges and in tunnels. We could show, how two different switch ways differ in their characteristic magnetic signals, which is an important feature for track-selective train localization. The train compass application was only suitable for coarse direction (two-way) if it is mounted with a certain distance to the tracks.

Future work will focus on algorithms for using magnetic field measurements. Nevertheless we think, that passive magnetic measurements will advance an approach in combination with other train-side sensors such as GNSS, IMU and a probabilistic data filter. Further research is necessary in the detailed influence of the presence of parallel tracks, other trains or coupled trains as well as certain elements of a railway switch and multiple sensor sets.

Acknowledgment

We want to thank the railway transportation company BRB ("Bayerische Regiobahn") for their cooperation with the measurement recordings.

References

[1] M. Lauer and D. Stein, "Algorithms and concepts for an onboard train localization system for safety-relevant services," in *Intelligent Rail Transportation (ICIRT), 2013 IEEE International Conference on*, Aug 2013.

[2] A. Acharya, S. Sadhu, and T. Ghoshal, "Train localization and parting detection using data fusion," *Transportation Research Part C: Emerging Technologies*, vol. 19, no. 1, pp. 75 – 84, 2011.

[3] O. Heirich, P. Robertson, and T. Strang, "RailSLAM - Localization of Rail Vehicles and Mapping of Geometric Railway Tracks," in *International Conference on Robotics and Automation, IEEE ICRA*, mai 2013.

[4] M. J. Caruso, C. H. Smith, T. Bratland, and R. Schneider, "A new perspective on magnetic field sensing," in *Sensors Expo Proceedings*, 1998.

[5] M. J. Caruso, "Applications of magnetic sensors for low cost compass systems," in *Position Location and Navigation Symposium, IEEE*, 2000, pp. 177–184.

[6] M. Angermann, M. Frassl, M. Doniec, B. Julian, and P. Robertson, "Characterization of the indoor magnetic field for applications in localization and mapping," in *Indoor Positioning and Indoor Navigation (IPIN), 2012 International Conference on*, Nov 2012, pp. 1–9.

[7] N. Wahlstrom, R. Hostettler, F. Gustafsson, and W. Birk, "Classification of driving direction in traffic surveillance using magnetometers," *Intelligent Transportation Systems, IEEE Transactions on*, vol. 15, no. 4, pp. 1405–1418, Aug 2014.

[8] T. Engelberg and F. Mesch, "Eddy current sensor system for non-contact speed and distance measurement of rail vehicles." *Computers in Railways VII, WIT Press: Southampton*, p. 1261 1270, 2000.

[9] A. Geistler, "Train location with eddy current sensors," in *CompRail, WIT Press*, June 2002.

[10] S. Hensel, C. Hasberg, and C. Stiller, "Probabilistic Rail Vehicle Localization With Eddy Current Sensors in Topological Maps," *Intelligent Transportation Systems, IEEE Transactions on*, vol. 12, no. 4, pp. 1525 –1536, dec. 2011.

[11] O. Heirich, P. Robertson, A. Cardalda Garcia, T. Strang, and A. Lehner, "Probabilistic localization method for trains," in *Intelligent Vehicles Symposium (IV), 2012 IEEE*, june 2012.

[12] A. Oppenheim, R. Schafer, and J. Buck, *Discrete-time signal processing*. Prentice Hall, 1999.

[13] National Geophysical Data Center: Magnetic field calculator. [Online]. Available: http://www.ngdc.noaa.gov/geomag-web/

[14] O. Heirich, A. Steingass, A. Lehner, and T. Strang, "Velocity and location information from onboard vibration measurements of rail vehicles," in *Information Fusion (FUSION), 2013 16th International Conference on*, July 2013.